Computation of periodic wave shoaling over barred-beaches in a fully nonlinear numerical wave tank

Stéphan T. Grilli[1] and Juan Horrillo

Department of Ocean Engineering, University of Rhode Island, Narragansett, RI 02882, USA

Abstract

A numerical wave tank based on fully nonlinear potential flow theory is used to calculate changes in local properties of periodic waves shoaling over barred-beaches. Results show that highly nonlinear wave decomposition phenomena occur over the bars. These are analyzed in detail and discussed in the paper.

Keywords : numerical wave tank, shallow water wave transformations, coastal engineering.

1 Introduction

Bars on beaches are very important topographic features for many coastal engineering problems. For sufficiently high incident waves, shallow berms, and steep side slopes, bars induce large wave modulations, mostly on their onshore side and, as a result, significant variations with depth of local wave parameters such as celerity c, height H, and front to back asymmetry s_2/s_1 (Fig. 1). As we will see, these modulations result from highly nonlinear wave decomposition phenomena which occur when waves propagate into the deeper water region beyond the bar.

Such decomposition phenomena have been well observed in the field (e.g., Byrne, 1969; Young, 1989) and in the laboratory (e.g., Beji and Battjes, 1993), over submerged obstacles, shelves, or bars. They were analyzed and modeled using weakly nonlinear and weakly dispersive Boussinesq equations (BE) (e.g., Freilich and Guza, 1984; Seabra-Santos et al., 1987) or low-order Stokes-type expansions (e.g., Massel, 1983; Rey, 1992; Rey et al., 1992). Driscoll et al. (1992) and Ohyama and Nadaoka (1994) used models based on Fully Nonlinear Potential Flow (FNPF) theory to calculate periodic wave propagation over submerged rectangular obstacles and showed that, for

[1]Distinguished Associate Professor, fax. : 1-401-874-6837; email : grilli@mistral.oce.uri.edu

large height to depth ratios over the obstacle, the strong nonlinearity in the wave field requires using a fully nonlinear method in which both wave shape and celerity are correctly calculated. This was also observed by Grilli et al. (1994) who studied the propagation of large solitary waves (breaking and non-breaking) over submerged trapezoidal breakwaters, using both a FNPF model and laboratory experiments. For waves propagating over steep obstacles on a flat bottom, Driscoll et al. (1992) and Ohyama and Nadaoka (1994) showed that higher harmonics are generated as bound waves in the shallower water region over the obstacle, and then released as free waves beyond the obstacle, where wave nonlinearity is weaker due to the deeper water depth. The initial harmonic generation depends on the dimensions of the obstacle (i.e., berm depth and width) and on incident wave period (i.e., wavelength) and height (i.e., incident steepness).

Grilli and Horrillo (1996,1997b) used a FNPF *Numerical Wave Tank* (NWT) to calculate nonlinear properties of periodic waves, of height H_o and period T in deep water, shoaling over "cylindrical beaches", with *monotonously decreasing and mildly sloping* depth variation $h(x)$. Their two-dimensional (2D) NWT combined (Grilli et al., 1989; Grilli and Subramanya, 1996; Grilli and Horrillo, 1997a) : (i) a higher-order Boundary Element (BEM) solution of Fully Nonlinear Potential Flow (FNPF) equations; (ii) an exact generation of finite amplitude periodic waves (*Streamfunction Waves*) at the deeper water extremity (Γ_{r1}); and (iii) an *Absorbing Beach* (AB) at the far end of the tank (featuring both free surface absorption on Γ_f and lateral active absorption on Γ_{r2}). A feedback procedure was developed to adaptively calibrate the beach absorption coefficient so as to absorb the period-averaged energy of waves entering the AB at $x = x_l$. After absorption of initial transient waves, computations in the NWT thus reached a *quasi-steady* state for which reflection from the AB was very small. Nonlinear properties of shoaling waves were calculated and validation tests were performed to assess their sensitivity to the AB location and to the resolution of the spatial discretization. Numerical results were also compared to laboratory experiments for periodic wave shoaling and propagation over a bar (Beji and Battjes, 1993). All the tests were found satisfactory.

Using the validated NWT, Grilli and Horrillo (1997b) (GH) calculated the shoaling of waves of various heights and periods over 1:35, 1:50, and 1:70 slopes, both plane and natural (i.e., with a bathymetry following Dean's (1991) equilibrium beach profile) , up to very close to the breaking point. Both local (H, c, L,...) and integral properties of shoaling waves were calculated and, due to the low reflection from the slope and the AB, found to be very repeatable for successive waves. For various mild slopes, nonlinear properties of waves of different height and period but same deep water steepness $k_o H_o$ were found to be almost identical for the same relative depth kh. In the shallower water region, linear, weakly nonlinear, and higher-order steady wave (Sobey and Bando, 1991) theories did not, in general, accurately predict shoaling wave properties, especially for $H/h > 0.15$. Linear wave theory (LWT; e.g., Dean and Dalrymple, 1984), in particular, was in error by up to 85% for the wave height and celerity at the breaking point. The weak nonlinearity and/or the lack of wave skewness in these theories were identified as the main sources of errors.

In this paper, the same methodology as in GH's study is applied to periodic waves shoaling over a barred-beach (Fig. 1). Physical features of periodic wave propagation over bars are first discussed in general, and then analyzed in detail.

2 General features of periodic wave propagation over bars

Fig. 1a shows a sketch of the NWT used in the present study. The base-profile for the beach has the shape of Dean's (1991) equilibrium beach profile, with a 1:50 average slope. A bar, with a 1:20 seaward and a 1:10 shoreward slope, and a crest with nondimensional depth 0.2, is located toward the top of the slope. [The geometry of this bar is similar to that of Beji and Battjes' (1993) experiments which GH used to validate their shoaling computations.] As in GH, since waves of moderate incident steepness initially behave as predicted by LWT, computations are initiated in intermediate water, in the deshoaling zone, at a depth $h_o^* = 0.6 h_o$. Corresponding wave characteristics in deep water (depth h_o) are back-calculated using LWT. Three incident waves of height $H_o'^* = H_o^*/h_o = 0.06$ and periods $T' = T\sqrt{g/h_o} = 5.5$, 6.5, and 7.5 are successively generated at Γ_{r1}, as exact finite amplitude zero-mass-flux streamfunction waves (Grilli and Horrillo, 1997a). General data for these three test waves are summarized in Table 1. An AB is specified in the NWT for $x' \geq x_l' = 30$, with a tapered bottom variation aimed at improving energy absorption (Grilli and Horrillo, 1997a); the depth at the AB's entrance is $h_l' = 0.1$, and $h_1' = 0.5$ at its extremity. Numerical data in the NWT (i.e., spatial and temporal discretizations) are selected for

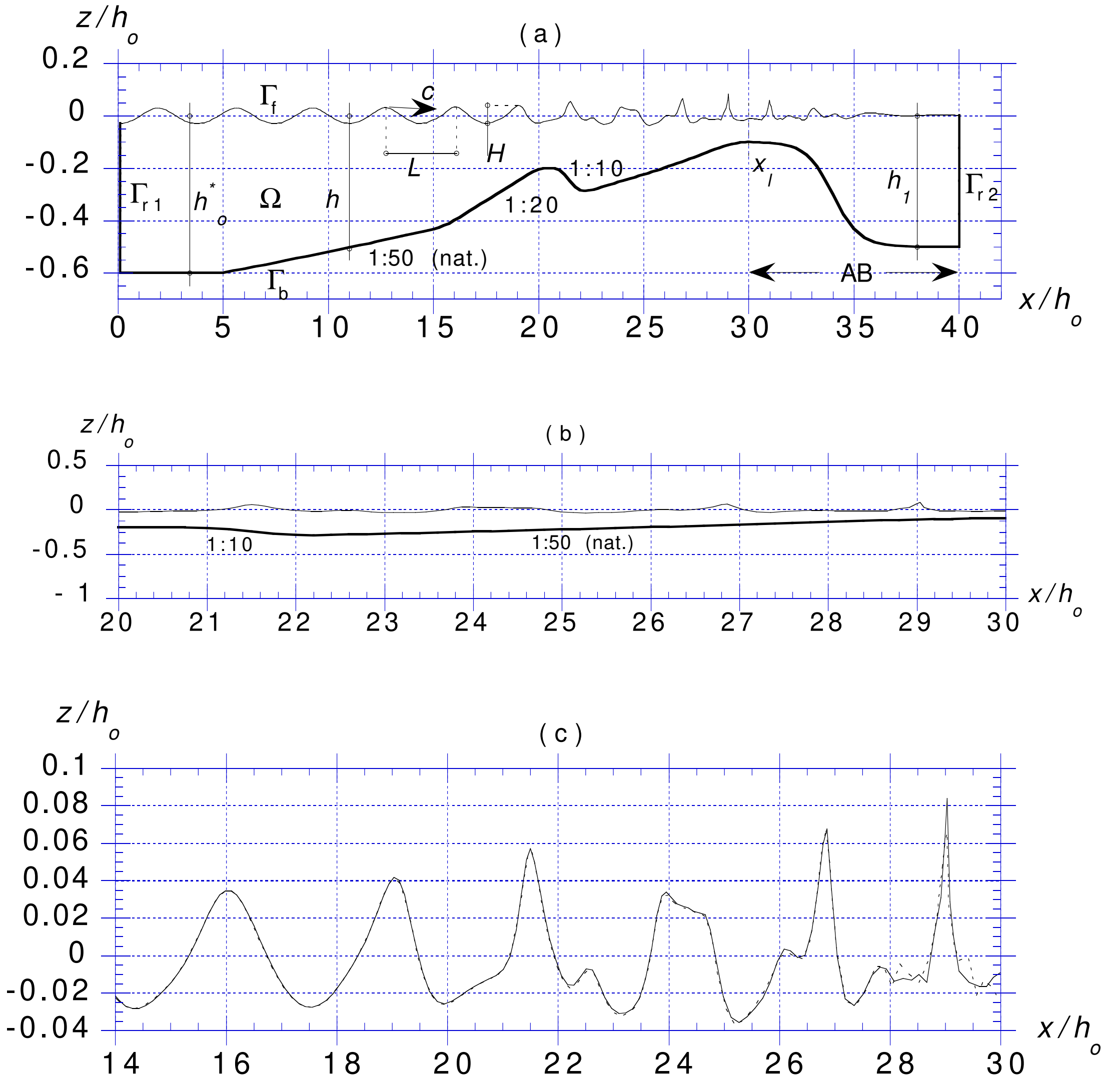

Figure 1: Sketch of computational domain and typical free surface elevation for 2D-FNPF computations of a periodic wave, of height H_o and period T in depth h_o, shoaling over a beach with Dean's equilibrium profile (1:50 average slope) and a bar. (a) NWT set-up. (b) Blow-up of free surface shape in undistorted scale (case 1, Table 1). (c) Free surface shape for case 1 (Table 1) at, $t' =$ (——) $15.75T'$; (- - - - -) $16.75T'$.

No.	H'_o	T'	H'^{*}_o	k'_o	$k_o h^*_o$	$k_o H_o$	c'_o	L'_o
1	0.0635	5.5	0.06	1.305	0.79	0.0852	0.8754	4.816
2	0.0626	6.5	0.06	0.934	0.56	0.0594	1.0345	6.724
3	0.0614	7.5	0.06	0.702	0.42	0.0361	1.1937	8.953

Table 1: Input characteristics of incident waves in the NWT : H'_o deep water wave height; T' wave period; H'^{*}_o initial wave height at depth $h'^{*}_o = 0.6$; $k'_o = (2\pi/T')^2$ (linear) deep water wave number; $k_o H_o$ initial wave steepness; $c'_o = T'/(2\pi)$, $L'_o = c'_o T$, the linear deep water wave celerity and wavelength. Dashes indicate nondimensional variables (length scale : h_o; time scale : $\sqrt{h_o/g}$, with g, the gravitational acceleration).

each case in order to ensure high accuracy of the computations.

A typical result for the calculated free surface shape is shown in Fig. 1, for case 1 (Table 1) at $t' = 86.64 = 15.75T'$ from the (cold) start of the computations. At this stage, the initial transient front has been absorbed in the AB and computations have reached a quasi-steady state. This is confirmed in Fig. 1c which shows two free surface profiles obtained at a one-period time interval : the two profiles are nearly identical, except for small high frequency oscillations close to the AB entrance ($x' > 28$). Seaward of the bar ($x' \leq 21$), wave shoaling appears qualitatively similar to that obtained for monotonous mild slopes (GH) : as waves propagate up the beach, their length reduces, their height increases, and their profile becomes increasingly front/back asymmetric (i.e., skewed), with higher and narrower crests, and longer and shallower troughs. Shoreward of the bar ($x' \geq 21$), however, the free surface profile appears very different from typical shoaling profiles, and decomposes into higher-frequency oscillations. Just before entering the AB, close to the breaking point ($x' \geq 28$), the waves somewhat recover the sawtooth/soliton-like shape typical of pre-breaking shoaling waves.

In the present study, which features a varying beach topography, when waves reach the bar, due to the initial shoaling over the mildly sloping base-profile of the beach, they are already significantly nonlinear, with a height about 45% of the local depth, and significant energy transferred to bound second and higher-order harmonics (this will be detailed in the following Section). Upon reaching the deeper water region behind the bar, wave nonlinearity drops and, as over a flat bottom, the higher harmonics are released as free waves. These free waves induce significant spatial modulations of the wave profile, quite apparent in Fig. 1, over some distance but, further onshore, as waves again propagate up the base-profile of the beach and depth decreases, shoaling re-occurs and, for sufficiently shallow depth, the free higher harmonics again become bound to the main wave and the wave profile more or less re-assumes a typical shoaling shape. Therefore, unlike with underwater obstacles over constant depth (as in, e.g., Driscoll et al., 1992) the modulation region shoreward of the bar is limited in extension by the reducing depth, clearly, as a function of incident wavelength, bar berm geometry, and beach slope. In the case of Fig. 1, the modulation region covers a horizontal distance of about 5-6h_o.

3 Detailed features of periodic wave propagation over bars

Results for the three wave propagation experiments in the NWT will now be detailed. More specifically, the variations of local wave parameters studied by GH over mild slopes (i.e., c, H/H_o, s_2/s_1) will be analyzed over the bar and in the modulation region beyond the bar where wave behavior becomes very irregular.

3.1 Surface elevation and wave harmonics

Figures 2, 3, and 4, parts a to c, show surface elevations calculated for cases 1 to 3 in Table 1, respectively, at three separate times taken over a one period interval after computations in the NWT have reached a quasi-steady state (this can easily be confirmed by comparing parts a and c of each figure). The plotted curves have been limited to the region directly above and beyond the bar, where the bar effect is most significant ($14 \leq x' \leq 30$). In each case, successive individual waves have been numbered in such a way that they can be followed as a function of time. Part d of the figures gives, for each case, the spatial variations of the first three normalized harmonic amplitudes ($2a_i/H_o; i = 1, 2, 3$). These were obtained from the Fourier transforms of time series of surface elevations taken at several "numerical gages" in the NWT.

The general picture presented in the previous Section is confirmed with, in each case, standard wave shoaling occurring prior to the bar and wave decomposition beyond the bar. As in GH, before the bar ($x' \leq 21$), wave energy is continuously transferred from the fundamental to bound higher-

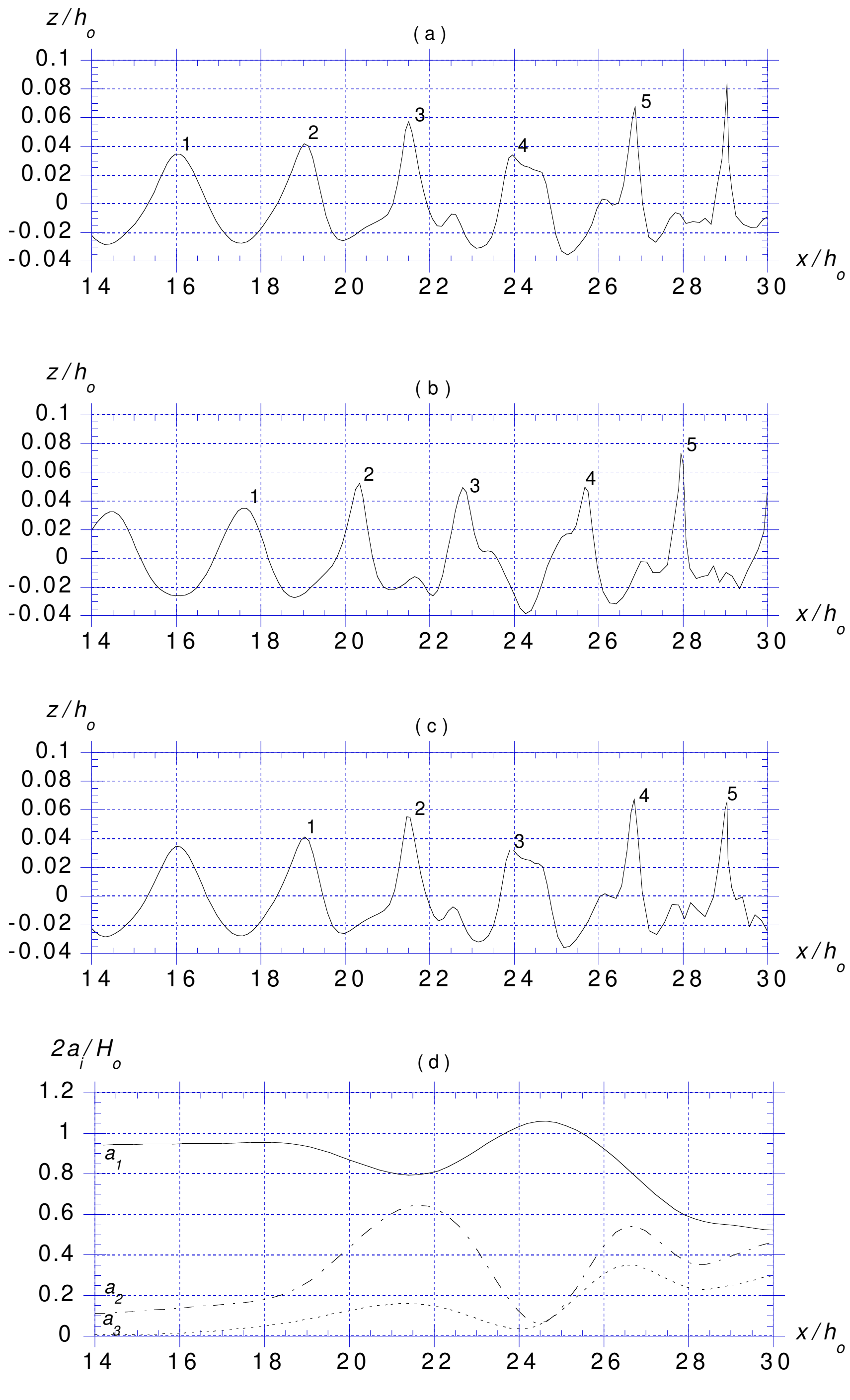

Figure 2: Computed surface elevations for case 1 (Table 1) at $t' =$ (a) $86.64 = 15.75T'$; (b) $89.38 = 16.25T'$; and (c) $92.13 = 16.75T'$. [Numbers on the figures identify specific waves at different times.] (d) First three normalized wave harmonics a_i.

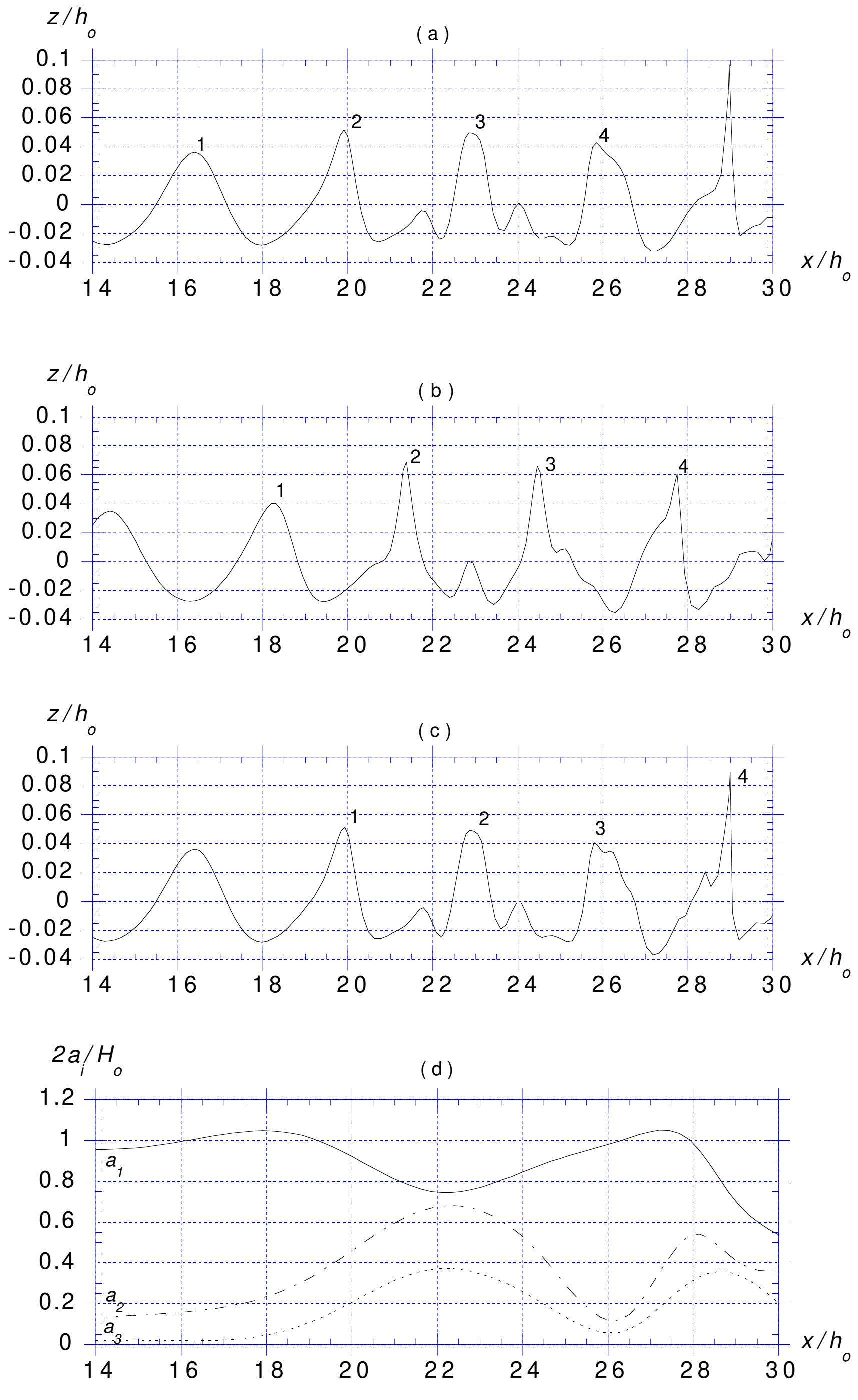

Figure 3: Computed surface elevations for case 2 (Table 1) at $t' =$ (a) $78.00 = 12T'$; (b) $81.26 = 12.5T'$; and (c) $84.5 = 13T'$. (d) First three normalized wave harmonics a_i.

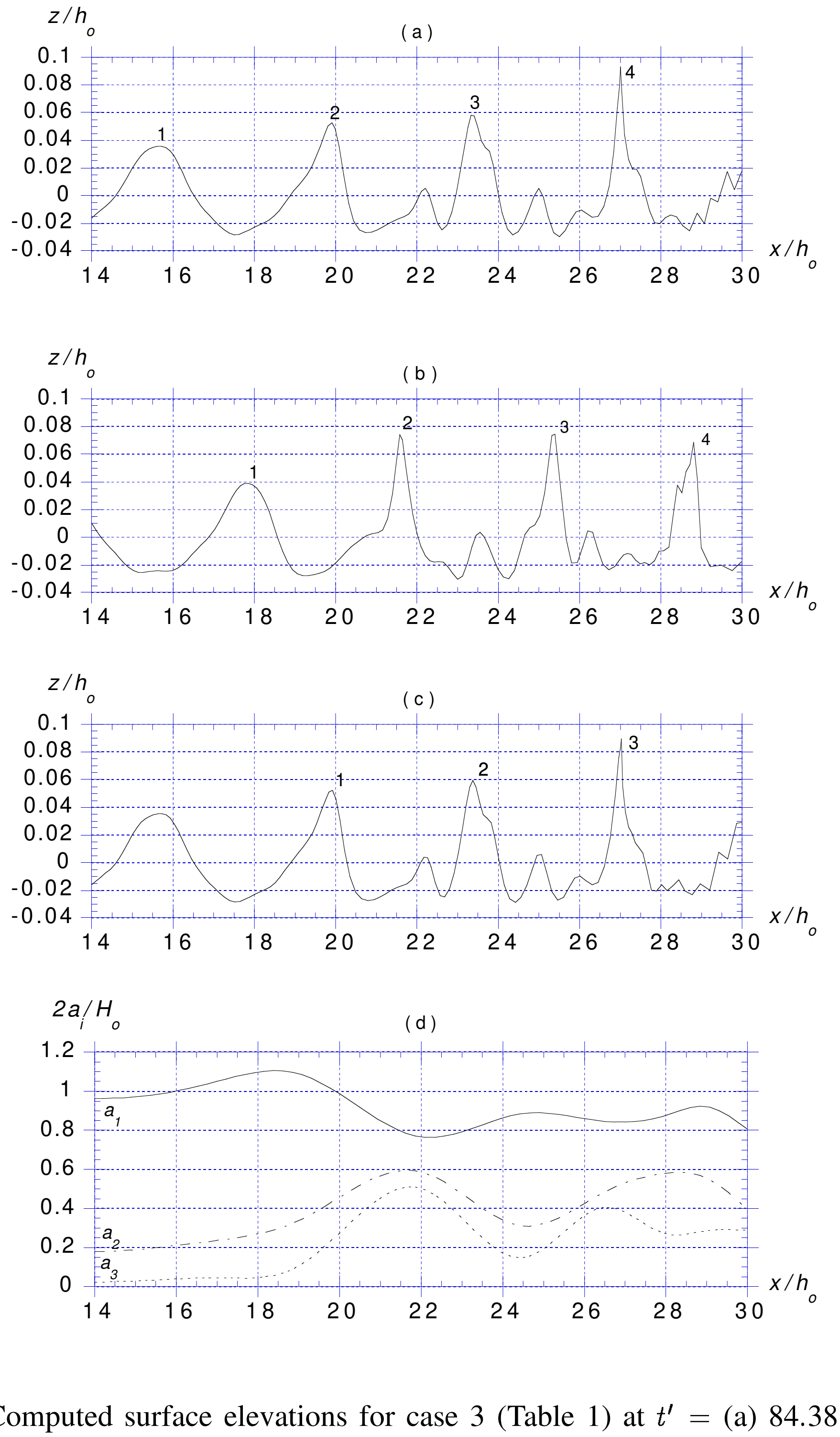

Figure 4: Computed surface elevations for case 3 (Table 1) at $t' =$ (a) $84.38 = 11.25T'$; (b) $88.13 = 11.75T'$; and (c) $91.88 = 12.25T'$. (d) First three normalized wave harmonics a_i.

order harmonics (the initial slight increase in a_1 is due to reflection by the slope). As a result, wave shape becomes increasingly skewed and sawtooth-like. Upon passing over the bar berm ($x' > 21$), waves reach the deeper water region beyond the bar and the harmonics are released as free waves. This results in marked oscillations in harmonic amplitudes and in strong spatial modulations of the wave profile. The modulation length for a_2 is approximately 4.8, 5.6, and $6.8h_o$, for each case, respectively, i.e., about twice the wavelength in the middle of the modulation region. For cases 1 and 2, waves re-assume their sawtooth-like shoaling shape before entering the AB ($x' \geq 30$), and the harmonic amplitudes seem to come back to a prolongation of what they were before reaching the bar. For case 3, the modulation region extends up to the AB.

3.2 Wave height

Fig. 5, parts a to c, shows normalized wave height variations calculated for cases 1,2 and 3 in Table 1, as $K_s = H/H_o$. In each figure, in addition to these results, both the FNPF wave height variation calculated for a 1:50 natural slope (i.e., the base-profile of the beach without a bar as in GH) and the wave height variation predicted by LWT for the barred-beach, have been plotted for comparison. For each case, the FNPF wave height variation for the barred-beach departs from that corresponding to the base-profile, upon reaching the bar berm. Toward the end of the modulation region beyond the bar, however, the barred-beach results seem to agree better with the latter. As expected from earlier studies, LWT significantly underpredict wave height.

In Fig. 5d, due to wave modulations, the FNPF height variations for the barred-beach are multiple-valued functions of relative depth $k_o h$ (whereas LWT gives superimposed single-valued results, as would also be the case for results of the base-profile). The patterns of wave height variations beyond the bar in the three cases show clear similarities.

3.3 Wave asymmetry

Fig. 6, parts a to c, shows normalized wave slopes calculated for cases 1 to 3 in Table 1, as $2s/\gamma_o$, with $\gamma_o = H_o/L_o$. For the back and front slopes of the wave, we have $s_1 = H/L_1$ and $s_2 = H/L_2$, respectively, where (L_1, L_2) denote distances between a crest and the previous and

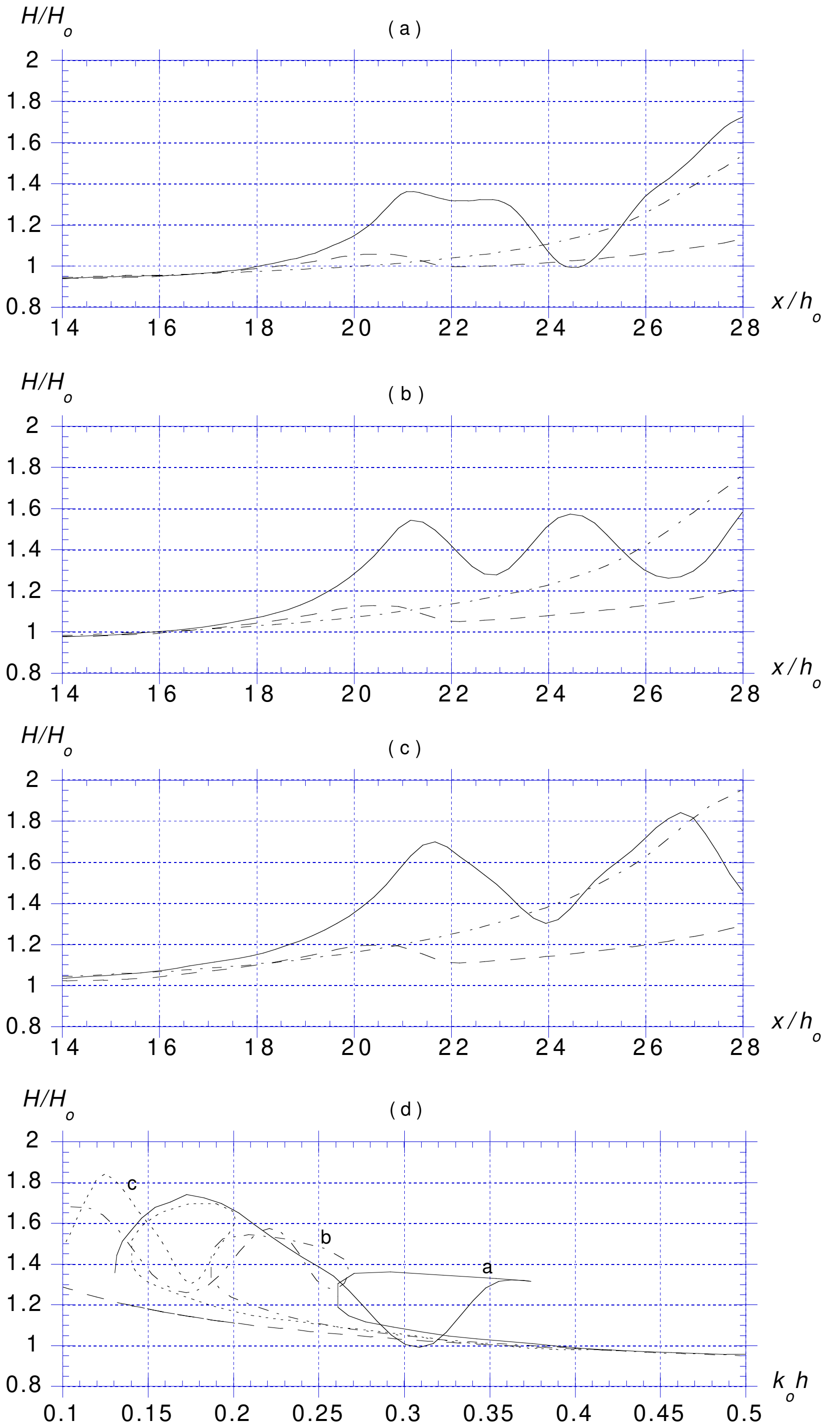

Figure 5: Computed wave height for cases (Table 1) : (a) 1; (b) 2; and (c) 3. (——) NWT computations for the barred-beach of Fig. 1; (– – –) LWT results for the same case; (– - –) NWT computations for the natural 1:50 base-profile (without a bar). Fig. (d) shows the NWT barred-beach results as a function of $k_o h$ for cases : (——) 1; (– - –) 2; and (- - - -) 3; (– – –) indicates LWT results.

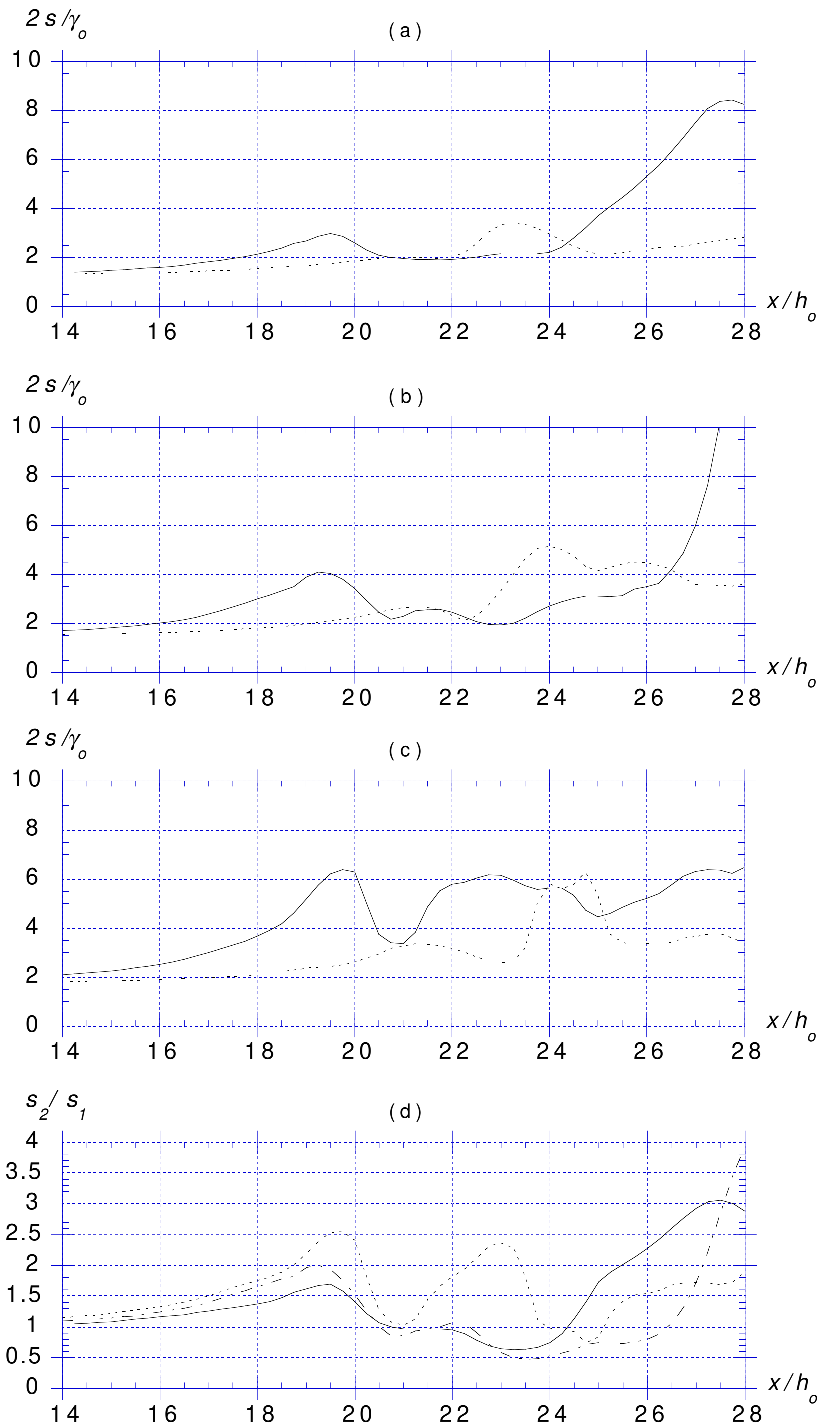

Figure 6: (a)-(c) : computed front (——) (s_2) and back (- - - -) (s_1) normalized wave slopes, for the barred-beach of Fig. 1 and cases (Table 1; $\gamma_o = H_o/L_o$) : (a) 1; (b) 2; and (c) 3. Fig. (d) shows the front/back asymmetry computed for cases : (——) 1; (– – –) 2; and (- - - -) 3.

next trough, respectively (a trough is defined as the point of minimum surface elevation between two successive crests in the wave train). Part d of Fig. 6 gives the ratio of front to back wave slopes, $s_2/s_1 = L_1/L_2$, i.e., a measure of wave front/back asymmetry.

In each case, prior to reaching the bar, both front and back slopes continuously increase due to shoaling, with a larger relative increase for the front slope than for the back slope, due to increasing wave skewness. As a result, the front/back asymmetry also continuously increases before the bar, from a value of 1 in deep water. For the beach base-profile, GH showed that this pattern is maintained up to reaching the AB. On the barred-beach, however, the modulations in wave shape beyond the bar induce significant changes in wave slopes. In each case, the wave front slope first reaches a maximum at around $x' = 19$, then drops over the bar berm and stabilizes beyond the bar, to finally increase again. The back slope keeps increasing over and beyond the berm and reaches a maximum at about 2.8, 4.3, and 4.7 h_o after the front slope reaches its maximum, in each case respectively; the back slope then drops until $x' = 25$ (where water depth is about equal to the bar berm depth) and then stabilizes.

In Fig. 6d, except for a backward shift in space of $1.5h_o$ or so (equal to the berm width), wave front/back asymmetry seems to correlate well with the variations of H/H_o in Fig. 5, in the spatial region over and beyond the bar.

3.4 Wave celerity

Fig. 7, parts a to c, shows normalized wave celerity c/c_o variations calculated for cases 1 to 3 in Table 1. In each figure, in addition to these results, both the FNPF wave celerity variation calculated for a 1:50 natural slope (i.e., the base-profile without a bar, as in GH) and the wave celerity variation predicted by LWT for the barred-beach, have been plotted for comparison. The FNPF wave celerity variation calculated for the 1:50 natural slope, and scaled for the depth variation of the barred-beach, has also been plotted.

For each case, the FNPF wave celerity variation for the barred-beach departs from that corresponding to the base-profile upon reaching the bar seaward slope. When corrected for depth, however, the latter results stay accurate until reaching the bar berm at $x' = 20$. This is because

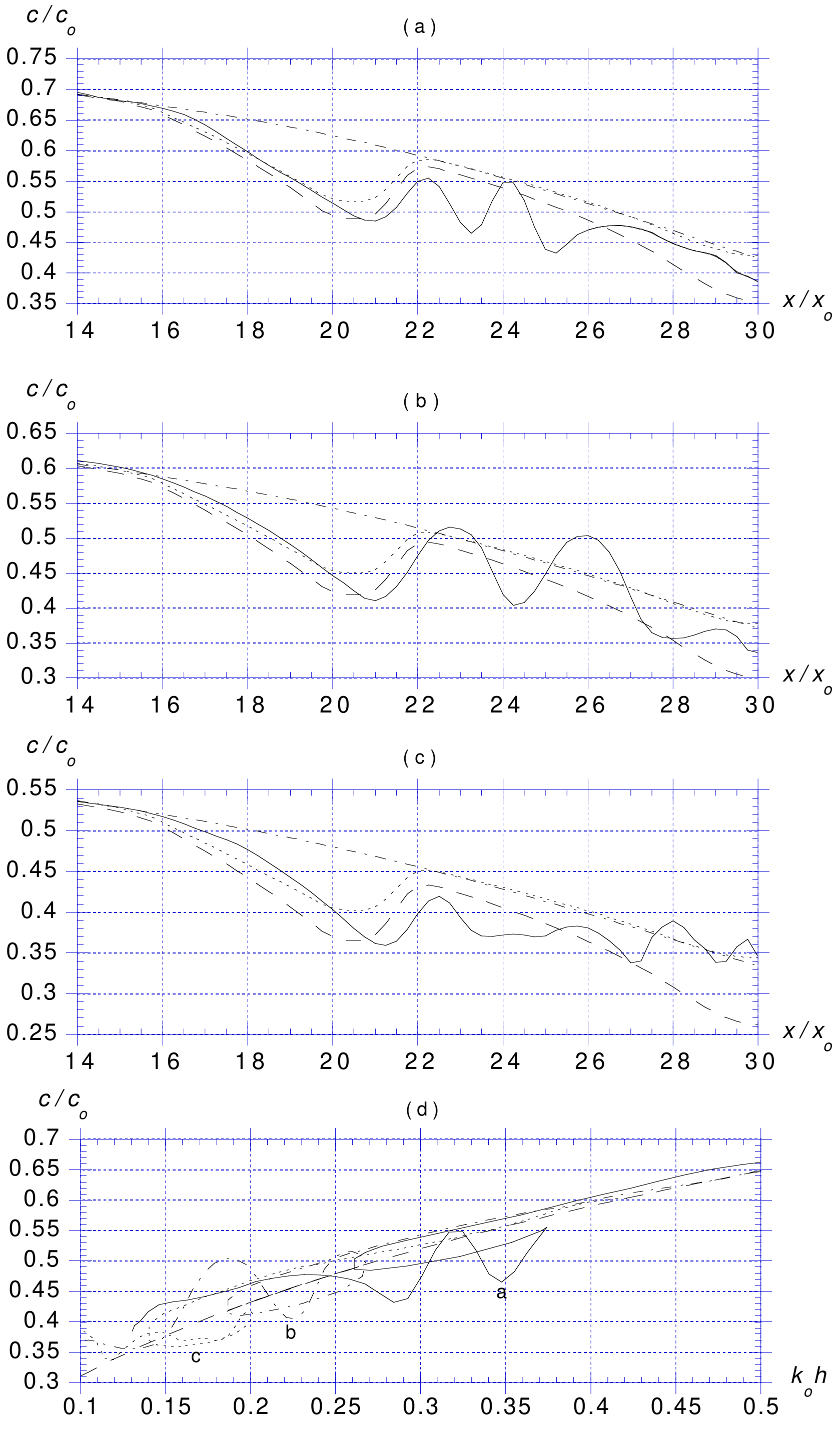

Figure 7: Computed wave celerity for cases (Table 1) : (a) 1; (b) 2; and (c) 3. (——) NWT computations for the barred-beach of Fig. 1; (– – –) LWT results for the same case; (– - –) NWT computations for the natural 1:50 base-profile (without a bar); (- - - -) application of the latter to the barred-beach. Fig. (d) shows the NWT barred-beach results as a function of $k_o h$ for cases : (——) 1; (– - –) 2; and (- - - -) 3; (– – –) indicates LWT results.

the 1:20 seaward slope is mild enough for the FNPF results, calculated for the same depth on the 1:50 natural slope, to apply in the present case. As expected from GH's study, in each case, LWT significantly underpredicts celerity before reaching the bar berm, and increasingly so, the longer the wave.

In each case, celerity increases over and beyond the bar, as a result of the increasing depth, and then strongly oscillates in the modulation region, due to changes in wave height inducing amplitude dispersion effects for the celerity. Finally, just before reaching the AB, wave celerity seems to stabilize and agree better with the FNPF results calculated for the base-profile without a bar. As expected, FNPF results calculated for the base-profile and corrected for depth do not capture the celerity oscillations in the modulation region. They also overpredict celerity over the bar berm. This is also the case for LWT.

In Fig. 7d, due to wave modulations, the FNPF celerity variations calculated for the barred-beach are multiple-valued functions of relative depth $k_o h$ (whereas LWT gives superimposed single-valued results, as would also be the case for results of the base-profile corrected for depth). Similarly to wave height, the patterns of wave celerity variations beyond the bar show clear similarities in the three cases.

3.5 Wave nonlinearity parameters

The results for wave shape and celerity variations over and beyond the bar show that highly nonlinear phenomena of wave decomposition, harmonic generation, and nonlinear exchanges of energy between harmonics occur and strongly affect wave parameters. A further confirmation of the strong nonlinearity is given in Fig. 8, parts a and b, where the typical nonlinearity parameters, $\delta = H/h$ and $\varepsilon = kH/2$, have been calculated for each case, as a function of x. Due to shoaling, the wave height to depth ratio δ already reaches a large 45 to 50% value over the bar, then drops beyond the bar, due to the increasing depth. For $x' > 25$, as shoaling re-occurs, δ starts increasing again to eventually reach $\mathcal{O}(1)$ values or more, before waves enter the AB. Similarly, wave steepness, ε, keeps increasing due to shoaling up to reaching a large 0.10 to 0.12 value at the bar; it then oscillates beyond the bar to finally increase again up to 0.12 to 0.17 (for comparison, the deep

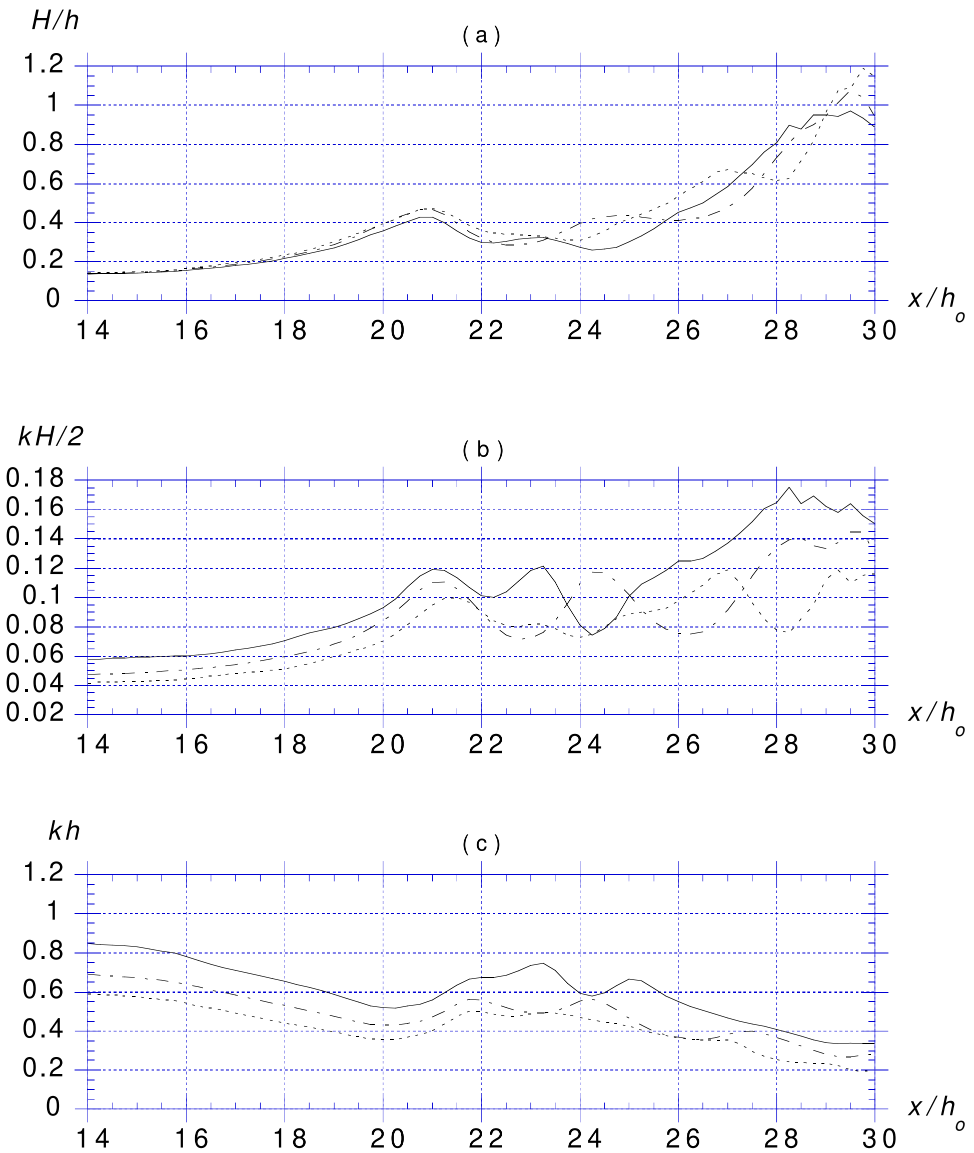

Figure 8: Wave nonlinearity parameters computed for the barred-beach of Fig. 1 and cases (Table 1) : (——) 1; (– – –) 2; and (- - - - -) 3.

water steepness of the limiting Stokes wave is $\varepsilon_{ol} = 0.221$).

In Fig. 8c, the shallowness parameter $\mu = kh$ has been plotted for each case, as a function of x. One sees that the large values of δ and ε calculated over the bar occur for intermediate water ($\pi \leq \mu \leq \pi/10$) and, hence, μ^2 cannot be considered to be very small either. In fact, waves only enter shallow water for $x' > 28$ or so.

4 Conclusions

Shoaling of three periodic waves with incident steepness $k_o H_o = 0.036$-0.085, over a barred-beach, was calculated in a 2D-FNPF-NWT. Results showed that : (i) prior to reaching the bar berm, *wave shoaling* occurs as observed over mild slopes by GH; (ii) for waves with large nonlinearity over the bar (such as here with $H/h = 0.45 - 0.50$), the increasing depth beyond the bar induces highly-nonlinear *wave decomposition* phenomena, with energy transfer between harmonics and the release of bound higher-harmonics into free waves; (iii) a *modulation region* appears beyond the bar, with a spatial extension function of the incident wave period/length, in which wave parameters such as celerity c, height H, and asymmetry s_2/s_1, become strongly oscillatory; in this region, c and H are *multiple-valued function* of depth $k_o h$; (iv) repetitive patterns of variations of wave *front and back slope* occur in the modulation region; (v) as *shoaling re-occurs* beyond the modulation region, waves eventually re-assume a shape and behavior similar to that observed over mildly sloping beaches; and (vi) the high value of wave *nonlinearity parameters*, δ and ε, over and beyond the bar requires using a fully nonlinear theory such as FNPF in the NWT, for an accurate computation of wave transformations.

Acknowledgements

This research work was sponsored by the US Naval Research Laboratory, Stennis Space Center, grants N-00014-95-1-G607 and N-00014-96-C012, from the Remote Sensing Division (code 7240).

References

Beji, S. and Battjes, J.A. (1993). "Experimental investigation of wave propagation over a bar," *Coastal Engng.*, Vol 19, pp 1-16.

Byrne, R.J. (1969). "Field occurrences of induced multiple gravity waves," *J. Geophys. Res.*, Vol 74, pp 2590-2596.

Dean, R.G. (1991). "Equilibrium beach profiles : characteristics and applications," *J. Coastal Res.*, Vol 7(1), pp 53-84.

Dean, R.G. and Dalrymple R.A. (1984). *Water Wave Mechanics for Engineers and Scientists*, Prentice-Hall.

Driscoll, A.M., Dalrymple, R.A. and Grilli, S.T. (1992). "Harmonic generation and transmission past a submerged rectangular obstacle," *Proc. 23rd Intl. Conf. on Coastal Engineering* (Venice, Italy), Vol 1, pp 1142-1152. ASCE edition.

Freilich, M.H. and Guza, R.T. (1984). "Nonlinear effects on shoaling surface gravity waves," *Proc. R. Soc. London*, Vol A311, pp 1-41.

Grilli, S.T. and Horrillo, J. (1996). "Fully nonlinear properties of periodic waves shoaling over slopes," *Proc. 25th Intl. Conf. on Coastal Engineering* (Orlando, Florida), Vol 1, pp 717-730. ASCE edition.

Grilli, S.T. and Horrillo, J. (1997a). "Numerical generation and absorption of fully nonlinear periodic waves," *J. Engng. Mech.*, Vol 123(10), pp 1060-1069.

Grilli, S.T. and Horrillo, J. (1997b). "Computation of properties of periodic waves shoaling over mild slopes in a fully nonlinear numerical wave tank," *J. Geophysical Res.* (submitted).

Grilli, S.T., Losada, M.A. and Martin, F. (1994). "Characteristics of solitary wave breaking induced by breakwaters," *J. Waterway, Port, Coastal, and Ocean Engng.*, Vol 120(1), pp 74-92.

Grilli, S.T., Skourup, J., and Svendsen, I.A. (1989). "An efficient boundary element method for nonlinear water waves," *Engng. Analysis with Boundary Elements*, Vol 6(2), pp 97-107.

Grilli, S.T. and Subramanya, R. (1996). "Numerical modeling of wave breaking induced by fixed or moving boundaries." *Computational Mech.*, Vol 17, pp 374-391.

Massel, S.R. (1983). "Harmonic generation by waves propagating over a submerged step," *Coastal Engng.*, Vol 7, pp 357-380.

Ohyama, T. and Nadaoka, K. (1994). "Transformation of a nonlinear wave train passing over a submerged shelf without breaking," *Coastal Engng.*, Vol 24, pp 1-22.

Rey, V. (1992). "Propagation and local behaviour of normally incident gravity waves over varying topography," *Eur. J. Mech. B: Fluids,* Vol 11, pp 213.

Rey, V., Belzons, M. and Guazzelli, E. (1992). "Propagation of surface gravity waves over a rectangular submerged bar," *J. Fluid Mech.*, Vol 235, pp 453.

Seabra-Santos, F.J., Renouard, D.P. and Temperville, A.M. (1987). "Numerical and experimental study of the transformation of a solitary wave over a shelf or isolated obstacle," *J. Fluid Mech.*, Vol 176, pp 117-134.

Sobey, R.J. and Bando, K. (1991). "Variations on higher-order shoaling," *J. Waterway Port Coastal and Ocean Engng.*, Vol 117(4), pp 348-368.

Young, I.R. (1989). "Wave transformation over coastal reefs," *J. Geophys. Res.*, Vol 94, pp 9779-9789.